HHS Public Access

Author manuscript

Magn Reson Imaging. Author manuscript; available in PMC 2017 November 01.

Published in final edited form as:

Magn Reson Imaging. 2016 November ; 34(9): 1248–1255. doi:10.1016/j.mri.2016.07.004.

Assessment of a Simplified Spin and Gradient Echo (sSAGE) Approach for Human Brain Tumor Perfusion Imaging

Ashley M. Stokes, PhD[1,2], **Jack T. Skinner, PhD**[1,3], **Thomas Yankeelov, PhD**[1,4], and **C. Chad Quarles, PhD**[1,*,2]

[1]Institute of Imaging Science, Vanderbilt University, 1161 21st Ave. S, Nashville Tennessee 37232, USA

Abstract

The goal of this study was to validate a simplified spin- and gradient-echo (sSAGE) approach to obtain T_1-corrected dynamic susceptibility contrast magnetic resonance imaging (DSC-MRI) data in a clinical brain tumor population. A five-echo SAGE sequence was used to acquire DSC-MRI data (n = 8 patients, 3 primary glioma, and 5 brain metastases). The ΔR_2^* and ΔR_2 time series obtained from a nonlinear fit of all echoes (SAGE) were compared to ΔR_2^* and ΔR_2 time series obtained analytically (sSAGE) using three echoes (two GE and one SE). Through the use of multiple echoes, both methods removed T_1 leakage effects from the ΔR_2^* and ΔR_2 time series, and the sSAGE ΔR_2^* and ΔR_2 time series were highly correlated with those from SAGE, with average correlations of 0.9. The resulting hemodynamic parameters included GE and SE cerebral blood volume (CBV), cerebral blood flow (CBF), mean vessel diameter (mVD), volume transfer constant (K^{trans}), and volume fraction of the extravascular extracellular space (v_e). For each metric, there was good correlation (>0.86) between sSAGE and SAGE, with no significant differences. The sSAGE method provides T_1-corrected GE and SE DSC-MRI parameters in an efficient and clinically feasible manner.

Keywords

dynamic susceptibility-contrast MRI; perfusion imaging; spin-echo and gradient-echo EPI; contrast agent leakage; permeability

[*]Corresponding author: C. Chad Quarles, Ph.D., Department of Imaging Research, Barrow Neurological Institute, St. Joseph's Hospital and Medical Center, 350 W. Thomas Rd, Phoenix Arizona 85013, USA, Christopher.Quarles@DignityHealth.org.

[2]Present Address: Department of Imaging Research, Barrow Neurological Institute, St. Joseph's Hospital and Medical Center, 350 W. Thomas Rd, Phoenix Arizona 85013, USA

[3]Present Address: National Comprehensive Cancer Network, 275 Commerce Drive, Suite 300, Fort Washington Pennsylvania 19034, USA

[4]Present Address: Department of Biomedical Engineering, Cockrell School of Engineering, The University of Texas at Austin, 107 W. Dean Keeton, BME Building, 1 University Station, C0800, Austin, Texas 78712

1. Introduction

Dynamic susceptibility-contrast magnetic resonance imaging (DSC-MRI) has the potential to report on vascular changes associated with tumor growth, as well as assess response to treatment. To maximize the contrast-to-noise ratio (CNR), clinical perfusion imaging often utilizes gradient echo (GE) sequences, which are sensitive to vessels of all sizes [1]. Spin echo (SE) sequences may provide complementary information due to their increased sensitivity to the microvasculature [2–5], at the cost of reduced CNR and signal-to-noise ratio (SNR) at longer echo times (TEs). Sequences that interrogate both GE and SE contrast simultaneously have been proposed, typically using a single GE and single SE sequence [6]. These combined sequences can provide a broad assessment of vascular parameters, including cerebral blood volume (CBV), cerebral blood flow (CBF), mean transit time (MTT), and mean vessel diameter (mVD) [1, 4, 6–9]. Unfortunately, these parameters cannot be reliably quantified with contrast agent (CA) extravasation [10–13], as is often the case in pathologies that involve a compromised blood-brain barrier (BBB), including brain tumors and stroke.

Under CA leakage, the most apparent sources of error are confounding T_1 leakage effects, although T_2 and T_2^* leakage effects are also known to adversely impact the perfusion parameters [13]. T_1 leakage effects typically manifest as higher post-bolus signal intensity and thus lower post-bolus ΔR_2^* (where $R_2^* = 1/T_2^*$). CBV, calculated from the integration of ΔR_2^*, is thus underestimated by T_1 leakage effects. Various methods have been utilized to minimize these T_1 leakage effects, including preload CA doses, pulse sequence optimizations, and post-processing correction methods [10–14]. A commonly used protocol involves a combination of a preload dose and post-processing correction using the Weisskoff method, which was previously shown to provide robust CBV estimates as validated by an intravascular iron oxide CA [11]. Alternatively, using a dual GE sequence [15], the signals from each echo can be combined to analytically remove the T_1 leakage effects, producing more robust perfusion parameters [13]. Although these methods have focused on GE perfusion parameters, SE and mVD metrics are similarly susceptible to T_1 leakage effects.

A combined spin- and gradient-echo (SAGE) method was proposed by Schmeideskamp et al. [4, 16] to provide T_1-insensitive perfusion measures using five echoes (two GE, two asymmetric SE, and a SE). We recently proposed a simplified SAGE (sSAGE) method that combines dual GE and a single SE (three total echoes) to similarly provide T_1-insensitive perfusion measures [17]. The original SAGE approach involves nonlinear fitting of the five echoes to a piecewise function to obtain T_1-insensitive R_2^* and R_2, which can be time-consuming. Alternatively, with the three-echo sSAGE method, T_1-insensitive ΔR_2^* and ΔR_2 time series can be computed analytically, thus precluding the need for nonlinear piecewise fitting. Instead, this method leverages the dual-gradient echo signal to correct the spin echo signal for T_1 leakage effects. This method was previously demonstrated in rat brain tumors on a preclinical system and compared with the full SAGE method [17]. For a rat brain with 1800 voxels and 200 repetitions, we found that the sSAGE method was over 450 times faster than the SAGE fitting. As the typical DSC acquisition in human brain has more than 25000 voxels, SAGE fitting could be prohibitive for routine clinical use. The sSAGE approach may be more practical in the clinical setting.

In the preclinical assessment of the simplified SAGE method, the sSAGE and SAGE methods showed similar DSC time series. Most importantly, no significant differences were found between the sSAGE- and SAGE-derived CBV measures, while single-echo CBV was significantly underestimated due to T_1 leakage effects. Based on the similar sSAGE and SAGE results observed in the preclinical assessment, the purpose of this study was to determine if sSAGE and SAGE provide similar results in a clinical study. Specifically, we aim to compare the sSAGE and SAGE sequences in human primary and metastatic brain tumors. As this approach only requires the acquisition and storage of three echoes and does not rely upon computationally demanding non-linear fitting algorithms, it could facilitate the more rapid clinical translation and adoption of SAGE-based DSC-MRI.

2. Methods

2.1 MRI Methods

MRI was performed at 3T (Achieva, Philips Healthcare, Best, Netherlands) using a 32-channel head coil (for high-grade glioma patients) or an 8-channel head coil (for brain metastases patients). The sSAGE- and SAGE-EPI sequences were used to obtain three and five echoes, respectively. Scan parameters were 1.8s repetition time (TR), field-of-view = 240 × 240 mm^2, voxel size = 3.16 × 3.16 × 5 mm^3 (reconstructed to 2.5 × 2.5 × 5 mm^3), number of echoes = 3 (sSAGE) or 5 (SAGE). Partial Fourier encoding and SENSE (acceleration factors 0.73 and 2.0, respectively) were used to obtain acceptable echo times. For the sSAGE acquisition, the 180° pulse follows immediately after the 2nd gradient echo, as the first $TE/2$ period determines the where the SE (echo 3) occurs. In the original SAGE acquisition, the SE (echo 5) is determined by the second $TE/2$ period, due to the acquisition of two asymmetric SE. The TEs were $TE_1 - TE_3$ = 8.6 / 26 / 85 ms for sSAGE and $TE_1 - TE_5$ = 8.8 / 26 / 55 / 72 / 90 ms for SAGE.

Prior to contrast administration, a pre-contrast T_1 map was acquired using a multi-flip angle approach (TR = 7.6 ms, TE = 4.6 ms, flip angle = 2°–20° in 2° increments). For the dynamic studies, 250 dynamics were acquired over 7.5 minutes. After 60 s of baseline images, 0.1 mmol/kg gadolinium-diethylenetriaminepentacetate (Gd-DTPA) was injected intravenously (infusion rate 4 ml/s, followed by 20 ml saline flush). Dynamic perfusion data were acquired with the full SAGE sequence in both primary brain tumor patients (n = 3, 42–55 years old, 2 males) and in metastatic brain tumor patients (n = 5, 47–72 years old, 2 males) (Table 1). All patient studies were performed in accordance with Vanderbilt University's Institutional Review Board (IRB) protocols.

2.2 Post-processing

To avoid differences that may occur between multiple injections, all perfusion data were acquired with the full SAGE sequence. The 2nd (GE) and 5th echo (SE) signals were used to determine the single-echo-based ΔR_2^* and ΔR_2 time series. The first two echoes (GE) were used to compute the T_1-insensitive sSAGE ΔR_2^* time series and the T_1-weighted signal (extrapolated to TE=0, $S_{TE=0}$), using Equations 1–2:

$$\Delta R_2^*(t)=\frac{1}{TE_2-TE_1}\left(\ln\left(\frac{S_{TE_2,\mathrm{pre}}}{S_{TE_2}(t)}\right)-\ln\left(\frac{S_{TE_1,\mathrm{pre}}}{S_{TE_1}(t)}\right)\right) \quad (1)$$

$$S_{TE=0}=S_{TE_1}\cdot\left(\frac{S_{TE_1}}{S_{TE2}}\right)^{TE_1/(TE_2-TE_1)}, \quad (2)$$

where $S_{TE1,pre}$ and $S_{TE2,pre}$ are the pre-bolus signals for TE_1 and TE_2, respectively, $S_{TE1}(t)$ and $S_{TE2}(t)$ are the dynamic signals from TE_1 and TE_2, respectively, and all other parameters are as defined above. As previously derived [17], the T_1-weighted signal was combined with the SE (Echo 5) to compute the T_1-insensitive sSAGE ΔR_2 time series from Equation 3:

$$\Delta R_2(t)=\frac{1}{TE_{SE}}\left(\ln\left(\frac{S_{TE_{SE},\mathrm{pre}}}{S_{TE_{SE}}(t)}\right)-\ln\left(\frac{S_{TE=0,\mathrm{pre}}}{S_{TE=0}(t)}\right)\right). \quad (3)$$

The SAGE-derived ΔR_2^* and ΔR_2 time-courses were obtained from all five echoes using nonlinear least squares fits to a piecewise function [16]. Briefly, the baseline signals were averaged to obtain the pre-bolus signal, and the voxel-wise R_2, R_2^*, signal intensity S^I_0, and γ were determined from Equation 4.

$$S(\tau)=\begin{cases} S_0^I\cdot e^{-\tau\cdot R_2^*} & 0<\tau<TE/2 \\ \frac{S_0^I}{\delta}\cdot e^{-TE\cdot(R_2^*-R_2)}\cdot e^{-\tau\cdot(2\cdot R_2-R_2^*)} & TE/2<\tau\le TE \end{cases}, \quad (4)$$

where γ is the slice profile mismatch between the excitation and refocusing pulses and was quantified using the mean pre-bolus signal [16]. Due to temporal inconsistencies previously observed with the full four-parameter fit, the slice profile mismatch γ was held constant for the dynamic time course [4, 17], yielding a reduced three-parameter fit. The dynamic perfusion data were fit with three parameters R_2, R_2^* and S^I_0 at each time point. $S^I_0(t)$ was the SAGE T_1-weighted signal, while the SAGE fits for $R_2^*(t)$ and $R_2(t)$ were used to determine the T_1-insensitive ΔR_2^* and ΔR_2 time series.

The arterial input function (AIF) was selected from the T_1-insensitive sSAGE ΔR_2^* time courses using an automated method [18] specifically adapted for use with multi-echo acquisitions [19]. The AIF was converted to CA concentration using a quadratic relationship [20]. The ΔR_2^* and ΔR_2 time-courses in tissue were converted to CA concentration using the effective transverse relaxivities (i.e., r_2^* and r_2) of Gd-DTPA; at 3T, r_2^* and r_2 were assumed to be 87 $mM^{-1}s^{-1}$ [20] and 20.4 $mM^{-1}s^{-1}$ [21]. GE and SE CBV were determined from the ratio of the scaled integrals of the tissue CA concentration curve and the arterial input function (AIF) curve. To avoid artifactually low CBV values that are often observed in

single-echo brain tumor data, negative CA concentrations were not included in the integration. CBF was taken as the maximum of the tissue impulse response function determined from the circular singular value decomposition of the AIF and tissue CA concentrations (23). Mean vessel diameter (mVD) maps were calculated from the ratio of the integrals of the single-echo, sSAGE and SAGE GE ΔR_2^* and SE ΔR_2 time series during bolus passage [1, 6, 7]. Each perfusion metric (rCBV, rCBF, and rmVD) is shown relative to the normal appearing white-matter ROI.

The pre-contrast T_1 map was combined with the T_1-weighted sSAGE and SAGE signals to produce ΔR_1 time series for each voxel [22, 23]. Using r_1 of 3.7 $mM^{-1}s^{-1}$ [24], the sSAGE and SAGE ΔR_1 were converted to CA concentration (C_t). As the AIF selection criteria for DSC and DCE often vary, a separate DCE-based AIF was obtained directly from the sSAGE C_t time series using previously published criteria [25]. DCE analysis was limited to tumor voxels exhibiting enhancement on the post-CA T_1-weighted image. Standard Tofts pharmacokinetic modeling of the sSAGE and SAGE C_t time series (250 dynamics) and the DCE-based AIF was performed to obtain maps of K^{trans} (CA transfer rate constant) and v_e (extracellular extravascular volume) [26, 27]. Voxels exhibiting non-physiological v_e values (>1) were excluded from analysis.

2.3 Statistical Analysis

To assess the similarity between the sSAGE and SAGE time series, Pearson's correlation coefficient (R) was used. For comparisons of ΔR_2^* and ΔR_2, the correlations were calculated using 40 points from 10s before injection to 60s after injection. For T_1-weighted signal comparisons, correlations were calculated using 220 points from 10 s before injection to the end of the acquisition (6.5 min after injection).

Regions of interest (ROIs) for tumor and normal appearing white matter were drawn on the T_1-weighted post-CA images. Group means were compared using a paired t-test with a 5% significance level. Concordance correlation coefficient (CCC) and Pearson's correlation coefficient (R) were used to assess agreement (accuracy and precision, respectively) between sSAGE and SAGE perfusion metrics across subjects.

3. Results

Figure 1 demonstrates representative dynamic DSC data in tumor ROIs from a primary glioma patient (left, a–c) and brain metastasis patient (right, d–f). In both cases, the single-echo ΔR_2^* and ΔR_2 (from echoes 2 and 5, respectively) are substantially reduced post-bolus (in some cases going below baseline) compared to sSAGE and SAGE due to T_1 leakage effects in the tumor tissue. The sSAGE and SAGE ΔR_2^* and ΔR_2 are inherently corrected for T_1 leakage effects and thus do not exhibit reduced post-bolus ΔR_2^* and ΔR_2. In addition, the sSAGE and SAGE time series for ΔR_2^*, ΔR_2, and T_1-weighted signal are in good agreement, with respect to shape and magnitude.

To quantify the similarity of the dynamic time series to the SAGE fits, Pearson's correlation coefficient R was calculated between sSAGE and SAGE for each patient. These correlations are shown in Table 1, along with patient demographic information. Overall, sSAGE ΔR_2^*

and ΔR_2 was consistently highly correlated with SAGE ΔR_2^* and ΔR_2. The average correlation was 0.92 (range 0.78–0.98) for ΔR_2^* and 0.90 (range 0.78–0.95) for ΔR_2. The sSAGE and SAGE T_1-weighted signals were also well correlated, with an average correlation of 0.89 (range 0.75–0.98).

The GE and SE CBV maps are shown in Figure 2 for single-echo (echoes 2 and 5), sSAGE and SAGE. Both single-echo CBV maps (GE and SE) are substantially underestimated in the tumor region (indicated by the white arrow), with mean rCBVs of 1.3 and 0.6, respectively. The sSAGE- and SAGE-derived maps exhibited similar higher CBV (rCBV = 2.05 and 1.99 for GE sSAGE and SAGE, respectively, and 1.78 and 1.80 for SE sSAGE and SAGE, respectively). Combining the GE and SE information, the mVD maps shown in Figure 2 are also similar between single echo, sSAGE, and SAGE (mVD = 1.8, 1.33 and 1.24, respectively). Finally, the K^{trans} maps obtained using the extracted ΔR_1 time series from sSAGE and SAGE are nearly identical (K^{trans} = 0.42 and 0.39, respectively).

Figure 3 demonstrates example voxel-wise correlation between SAGE and sSAGE rCBV in whole tumor ROIs in a primary glioma patient (left) and brain metastases patient (right). Both the GE and SE sSAGE rCBV fall along to the line of unity, indicating agreement with GE and SE SAGE rCBV.

The bar plots in Figure 4 show mean pooled CBV, CBF, and mVD in tumor relative to normal tissue using sSAGE and SAGE ΔR_2^* and ΔR_2 (n = 8; 3 glioma and 5 brain metastases). There were no significant differences observed between sSAGE and SAGE for GE and SE CBV ($p = 0.686$ and 0.128, respectively), GE and SE CBF ($p = 0.897$ and 0.52, respectively), mVD ($p = 0.566$), K^{trans} ($p = 0.116$), and v_e ($p = 0.779$).

The correlation plots between sSAGE and SAGE are shown in Figure 5. Both patient groups are shown in each plot, with filled markers for glioma patients (n = 3) and open markers for brain metastases patients (n = 5). For every metric tested, the linear correlation was highly significant ($p < 0.01$), with high CCC and R. The CCC was greater than 0.86 for each metric, while R was greater than 0.88 for all metrics.

Figure 6 shows the Bland-Altman mean-difference plots for each metric between sSAGE and SAGE. Almost no bias was observed for GE CBV, GE and SE CBF, mVD, and v_e. A slight negative bias was observed for SE CBV, and a slight positive bias was observed for K^{trans}. There were no obvious effects of tumor type (glioma versus brain metastases) on the relative bias in each metric.

4. Discussion

In this study, the three-echo sSAGE analytic approach was compared to a five-echo SAGE fitting approach in patients with primary glioma and brain metastases. A pooled analysis found no significant differences in any metric between sSAGE and SAGE. Each sSAGE and SAGE metric was well correlated, with high CCC and Pearson's R values. In addition, the similarity between sSAGE- and SAGE-based metrics held for both tumor types. Our results indicate that sSAGE can be used to reliably obtain T_1-corrected SE and GE perfusion measures.

Leakage correction methods often focus on minimizing T_1 effects, as they typically dominate single-echo data. In addition to T_1 effects, contrast agent leakage can also manifest as T_2^* (or T_2) effects. T_2^* and T_2 effects result from altered susceptibility differences between the intravascular space, extravascular extracellular space, and intracellular space. Although correcting for both effects is important to obtain reliable CBV, this is complicated in single-echo data that simultaneously exhibits competing T_1 and T_2^* or T_2 leakage effects [13, 28]. The advantage of the dual-echo approach is that it completely removes T_1 leakage effects analytically, rather than simply minimizing them. The sSAGE approach further extends this analytic approach to remove T_1 leakage effects from SE data. Once these effects are separated, the data can be corrected for T_2 and T_2^* leakage effect using an appropriate pharmacokinetic or biophysical model [10, 11, 29, 30].

The original SAGE approach removes T_1 leakage effects from ΔR_2^* and ΔR_2 data by quantifying the absolute T_2^* and T_2 values [4]. One limitation of the sSAGE approach is that absolute T_2^* and T_2 values are not obtained; however, as DSC-MRI relies on ΔR_2^* and ΔR_2 to obtain perfusion metrics, absolute values are not needed. Furthermore, for clinical implementation, computationally efficient methods to remove T_1 leakage effects are needed. As the SAGE approach relies on nonlinear piece-wise fitting of the five echoes, the computation time grows quickly with repetitions and brain voxels. For example, on a computer with a 2.8 GHz quad-core processor and 16 GB of RAM, the computation time for deriving the ΔR_2^* and ΔR_2 SAGE time series for a single human brain slice (approximately 3000 voxels with 170 repetitions) was 3.5 hours. For sSAGE, total calculation times of approximately 1 second were obtained for an entire human brain volume (15 slices) and all repetitions.

There are several limitations of this study. In accordance with our protocol, only one injection was permitted per patient, precluding our ability to perform DSC with both the sSAGE and SAGE sequences. However, the benefit of this approach is that prevents differences that may occur with multiple injections. Multiple injections would also alter the extent of the T_1 leakage effects, where the first injection would act as a preload dose. A second limitation is that there were a limited number of patients in each cohort, though significant differences were still observed. For the purpose of this study, a relatively small patient population is sufficient. The final limitation is that we did not correct for T_2^* leakage effects, which will ultimately be necessary to obtain more accurate measures of rCBV. However, this is outside the scope of the present study and will be the subject of future investigations.

In conclusion, this study validates an analytic approach to obtain T_1-insensitive hemodynamic parameters, including GE and SE CBV and CBF, mVD, K^{trans}, and v_e, in a human patient population. The data can be acquired using a three-echo simplified SAGE sequence with comparable results to the five-echo SAGE sequence. The analysis of sSAGE data is substantially faster than nonlinear fitting of the five-echo SAGE data, making it a more clinically feasible method to obtain T_1-corrected data. SAGE-based approaches, including both the full and simplified versions, provide a wealth of information about tumor vascularity, vessel size, and permeability, within a single scan acquisition.

Acknowledgments

We would like to thank Ryan Robison, PhD, for implementing the full SAGE sequence and Drs. Paul Moots, MD, and Anuradha (Bapsi) Chakravarthy, MD, for their collaboration. This work was performed at the Vanderbilt University Institute of Imaging Science, with support from NIH/NCI 1R01CA158079 and T.E.Y.'s Ingram Professorship.

References

1. Dennie J, Mandeville JB, Boxerman JL, Packard SD, Rosen BR, Weisskoff RM. NMR imaging of changes in vascular morphology due to tumor angiogenesis. Magn Reson Med. 1998; 40:793–799. [PubMed: 9840821]
2. Boxerman JL, Hamberg LM, Rosen BR, Weisskoff RM. MR contrast due to intravascular magnetic susceptibility perturbations. Magn Reson Med. 1995; 34:555–566. [PubMed: 8524024]
3. Kiselev VG, Strecker R, Ziyeh S, Speck O, Hennig J. Vessel size imaging in humans. Magn Reson Med. 2005; 53:553–563. [PubMed: 15723391]
4. Schmiedeskamp H, Straka M, Newbould RD, Zaharchuk G, Andre JB, Olivot JM, et al. Combined spin- and gradient-echo perfusion-weighted imaging. Magn Reson Med. 2012; 68:30–40. [PubMed: 22114040]
5. Troprès I, Grimault S, Vaeth A, Grillon E, Julien C, Payen J-F, et al. Vessel size imaging. Magn Reson Med. 2001; 45:397–408. [PubMed: 11241696]
6. Schmainda KM, Rand SD, Joseph AM, Lund R, Ward BD, Pathak AP, et al. Characterization of a first-pass gradient-echo spin-echo method to predict brain tumor grade and angiogenesis. Am J Neuroradiol. 2004; 25:1524–1532. [PubMed: 15502131]
7. Donahue KM, Krouwer HGJ, Rand SD, Pathak AP, Marszalkowski CS, Censky SC, et al. Utility of simultaneously acquired gradient-echo and spin-echo cerebral blood volume and morphology maps in brain tumor patients. Magn Reson Med. 2000; 43:845–853. [PubMed: 10861879]
8. Lemasson B, Valable S, Farion R, Krainik A, Remy C, Barbier EL. In vivo imaging of vessel diameter, size, and density: a comparative study between MRI and histology. Magn Reson Med. 2013; 69:18–26. [PubMed: 22431289]
9. Pannetier N, Lemasson B, Christen T, Tachrount M, Tropres I, Farion R, et al. Vessel size index measurements in a rat model of glioma: comparison of the dynamic (Gd) and steady-state (iron-oxide) susceptibility contrast MRI approaches. Nmr Biomed. 2012; 25:218–226. [PubMed: 21751270]
10. Bjornerud A, Sorensen AG, Mouridsen K, Emblem KE. T1- and T2*-dominant extravasation correction in DSC-MRI: part I--theoretical considerations and implications for assessment of tumor hemodynamic properties. Journal of cerebral blood flow and metabolism : official journal of the International Society of Cerebral Blood Flow and Metabolism. 2011; 31:2041–2053.
11. Boxerman JL, Prah DE, Paulson ES, Machan JT, Bedekar D, Schmainda KM. The Role of preload and leakage correction in gadolinium-based cerebral blood volume estimation determined by comparison with MION as a criterion standard. AJNR. American journal of neuroradiology. 2012; 33:1081–1087. [PubMed: 22322605]
12. Boxerman JL, Schmainda KM, Weisskoff RM. Relative Cerebral Blood Volume Maps Corrected for Contrast Agent Extravasation Significantly Correlate with Glioma Tumor Grade, Whereas Uncorrected Maps Do Not. Am J Neuroradiol. 2006; 27:859–867. [PubMed: 16611779]
13. Paulson ES, Schmainda KM. Comparison of Dynamic Susceptibility-weighted Contrast-enhanced MR Methods: Recommendations for Measuring Relative Cerebral Blood Volume in Brain Tumors. Radiology. 2008; 249:601–613. [PubMed: 18780827]
14. Quarles CC, Ward BD, Schmainda KM. Improving the reliability of obtaining tumor hemodynamic parameters in the presence of contrast agent extravasation. Magn Reson Med. 2005; 53:1307–1316. [PubMed: 15906288]
15. Vonken, E-jPA.; van Osch, MJP.; Bakker, CJG.; Viergever, MA. Simultaneous quantitative cerebral perfusion and Gd-DTPA extravasation measurement with dual-echo dynamic susceptibility contrast MRI. Magn Reson Med. 2000; 43:820–827. [PubMed: 10861876]

16. Schmiedeskamp H, Straka M, Bammer R. Compensation of slice profile mismatch in combined spin- and gradient-echo echo-planar imaging pulse sequences. Magn Reson Med. 2012; 67:378–388. [PubMed: 21858858]
17. Stokes AM, Quarles CC. A simplified spin and gradient echo approach for brain tumor perfusion imaging. Magn Reson Med. 2016; 75:356–362. [PubMed: 25753958]
18. Carroll TJ, Rowley HA, Haughton VM. Automatic Calculation of the Arterial Input Function for Cerebral Perfusion Imaging with MR Imaging1. Radiology. 2003; 227:593–600. [PubMed: 12663823]
19. Newton AT, Pruthi S, Stokes AM, Skinner JT, Quarles CC. Improving Perfusion Measurement in DSC-MRI Through the Use of Multi-echo Information for AIF Determination. AJNR. American journal of neuroradiology. in press.
20. Kjolby BF, Ostergaard L, Kiselev VG. Theoretical model of intravascular paramagnetic tracers effect on tissue relaxation. Magn Reson Med. 2006; 56:187–197. [PubMed: 16724299]
21. Skinner JT, Robison RK, Elder CP, Newton AT, Damon BM, Quarles CC. Evaluation of a multiple spin- and gradient-echo (SAGE) EPI acquisition with SENSE acceleration: applications for perfusion imaging in and outside the brain. Magn Reson Imaging. 2014; 32:1171–1180. [PubMed: 25179133]
22. Landis CS, Li X, Telang FW, Coderre JA, Micca PL, Rooney WD, et al. Determination of the MRI contrast agent concentration time course in vivo following bolus injection: Effect of equilibrium transcytolemmal water exchange. Magn Reson Med. 2000; 44:563–574. [PubMed: 11025512]
23. Stokes AM, Skinner JT, Quarles CC. Assessment of a combined spin- and gradient-echo (SAGE) DSC-MRI method for preclinical neuroimaging. Magn Reson Imaging. 2014; 32:1181–1190. [PubMed: 25172987]
24. Rohrer M, Bauer H, Mintorovitch J, Requardt M, Weinmann H-J. Comparison of Magnetic Properties of MRI Contrast Media Solutions at Different Magnetic Field Strengths. Investigative Radiology. 2005; 40:715–724. [PubMed: 16230904]
25. Li X, Welch EB, Arlinghaus LR, Chakravarthy AB, Xu L, Farley J, et al. A novel AIF tracking method and comparison of DCE-MRI parameters using individual and population-based AIFs in human breast cancer. Physics in medicine and biology. 2011; 56:5753–5769. [PubMed: 21841212]
26. Tofts PS. Modeling tracer kinetics in dynamic Gd-DTPA MR imaging. Journal of Magnetic Resonance Imaging. 1997; 7:91–101. [PubMed: 9039598]
27. Tofts PS, Brix G, Buckley DL, Evelhoch JL, Henderson E, Knopp MV, et al. Estimating kinetic parameters from dynamic contrast-enhanced t1-weighted MRI of a diffusable tracer: Standardized quantities and symbols. Journal of Magnetic Resonance Imaging. 1999; 10:223–232. [PubMed: 10508281]
28. Johnson G, Wetzel SG, Cha S, Babb J, Tofts PS. Measuring blood volume and vascular transfer constant from dynamic, T(2)*-weighted contrast-enhanced MRI. Magn Reson Med. 2004; 51:961–968. [PubMed: 15122678]
29. Schmiedeskamp H, Andre JB, Straka M, Christen T, Nagpal S, Recht L, et al. Simultaneous perfusion and permeability measurements using combined spin- and gradient-echo MRI. Journal of cerebral blood flow and metabolism : official journal of the International Society of Cerebral Blood Flow and Metabolism. 2013; 33:732–743.
30. Stokes AM, Semmineh N, Quarles CC. Validation of a T1 and T2* leakage correction method based on multiecho dynamic susceptibility contrast MRI using MION as a reference standard. Magn Reson Med. 2015 n/a-n/a.

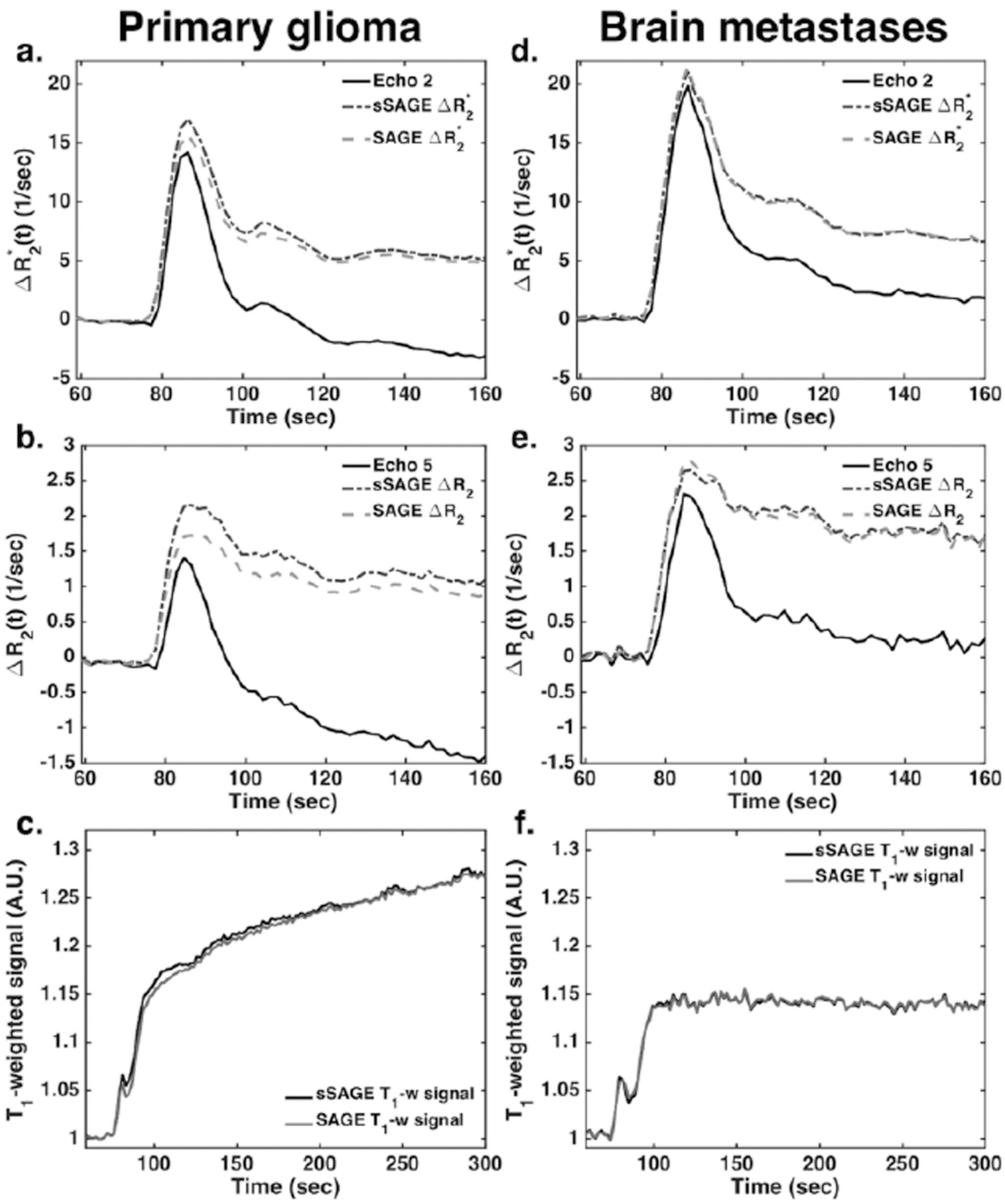

Figure 1.

Dynamic ΔR_2^* (a,b) and ΔR_2 (c,d) time series for a tumor ROI in a primary glioma patient (a–c) and brain metastases patient (d–f) following bolus injection of 0.1 mmol/kg Gd-DTPA. The sSAGE and SAGE-based T_1-weighted signals in a tumor ROI are also shown for each patient (c,f). In each case, the sSAGE and SAGE measures are similar, while the single-echo time-series are much lower, particularly at time points following the first pass of the contrast agent.

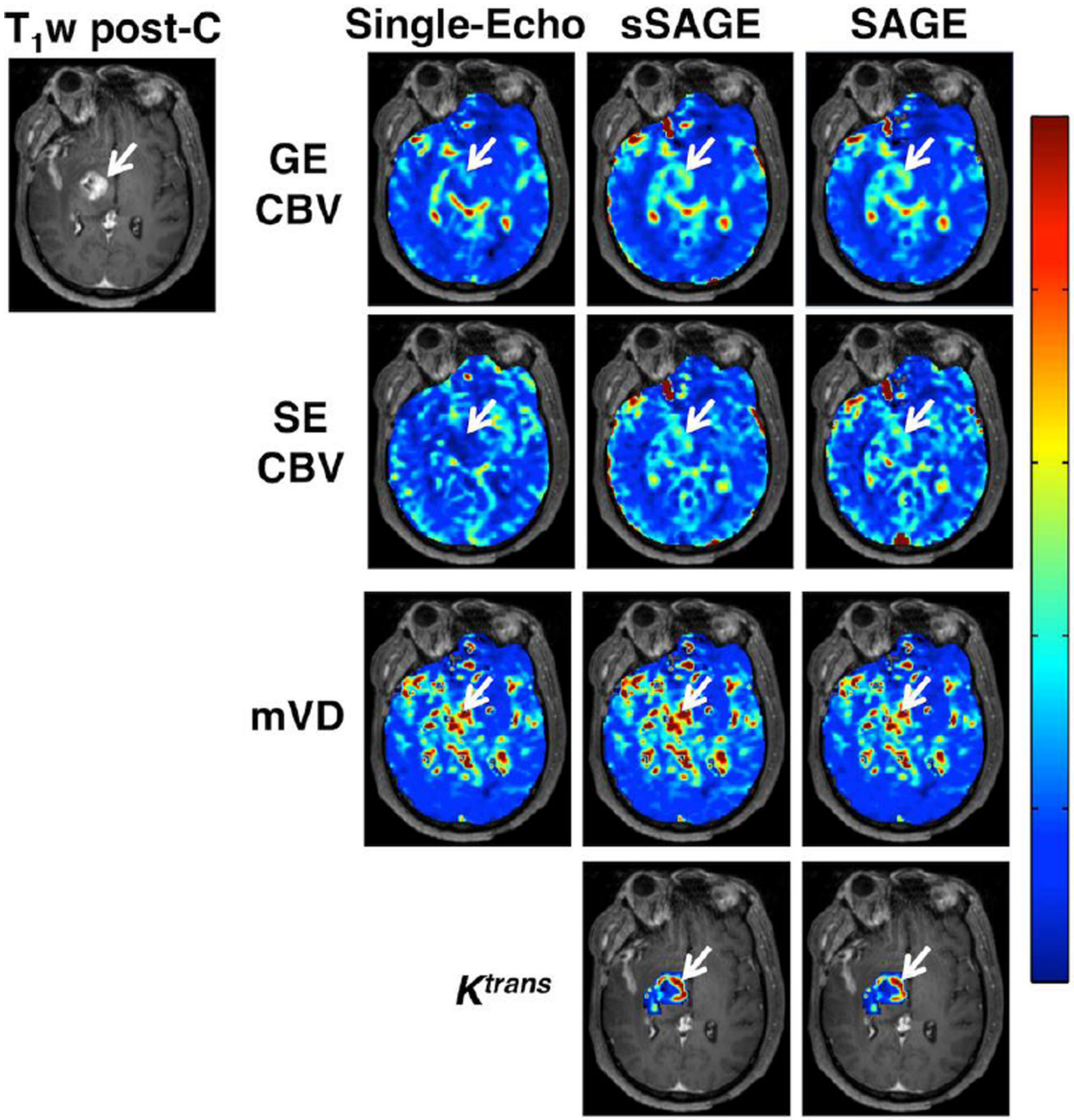

Figure 2.

DSC-MRI maps of GE CBV, SE CBV, mVD, and K^{trans} in a primary glioma patient (T_1-weighted post-contrast image shows tumor edge, indicated by arrow). The single-echo GE and SE CBV is lower than the sSAGE- and SAGE-based CBV, which showed similar results. There was little difference in mVD between single-echo, sSAGE, and SAGE in this patient. The sSAGE and SAGE derived K^{trans} maps showed good agreement.

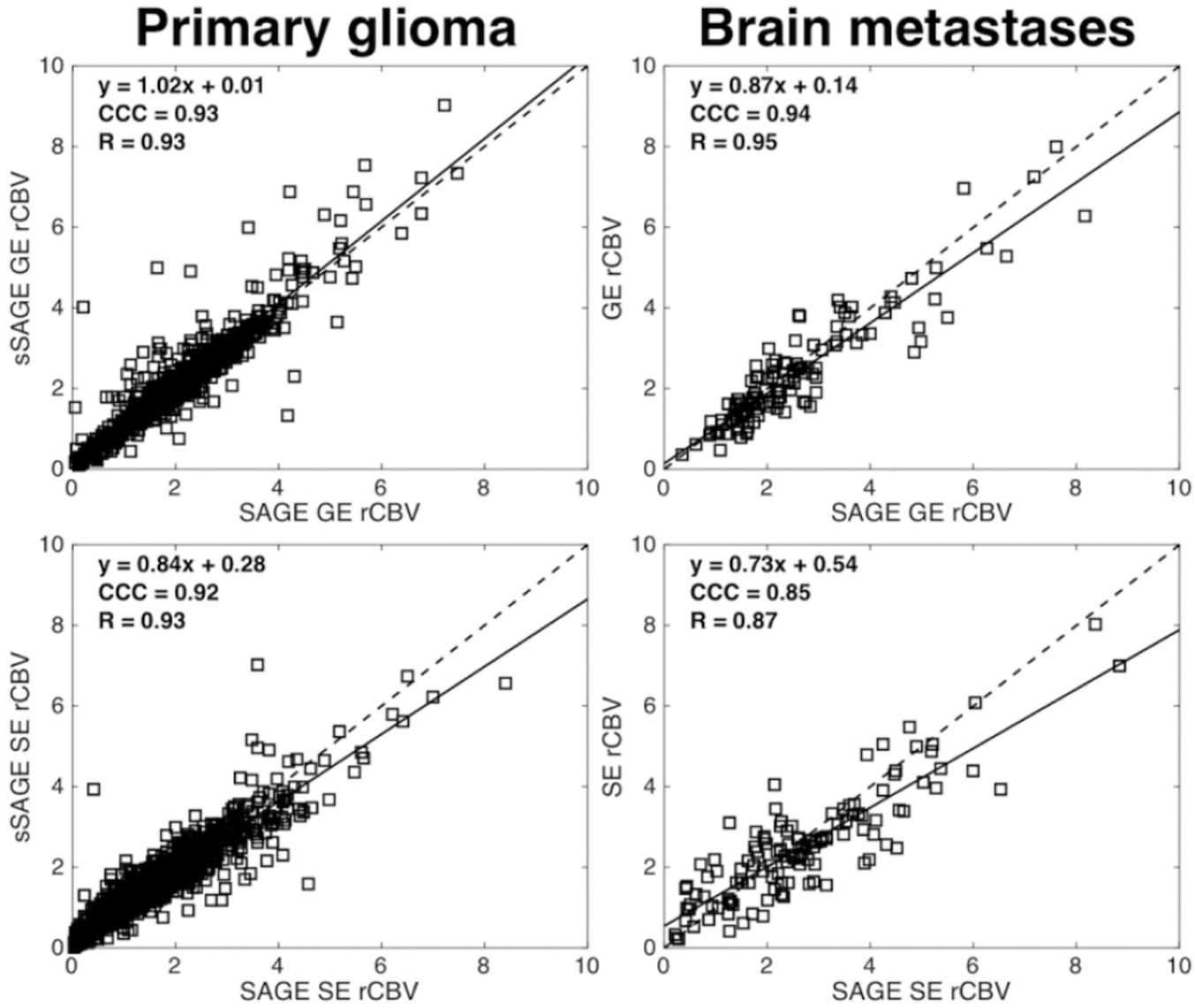

Figure 3.

Voxel-wise correlation plots between sSAGE and SAGE for GE rCBV (top) and SE rCBV (bottom) in a primary glioma patient (left) and brain metastases patient (right). Within a single patient, sSAGE and SAGE estimates of GE and SE CBV showed good agreement.

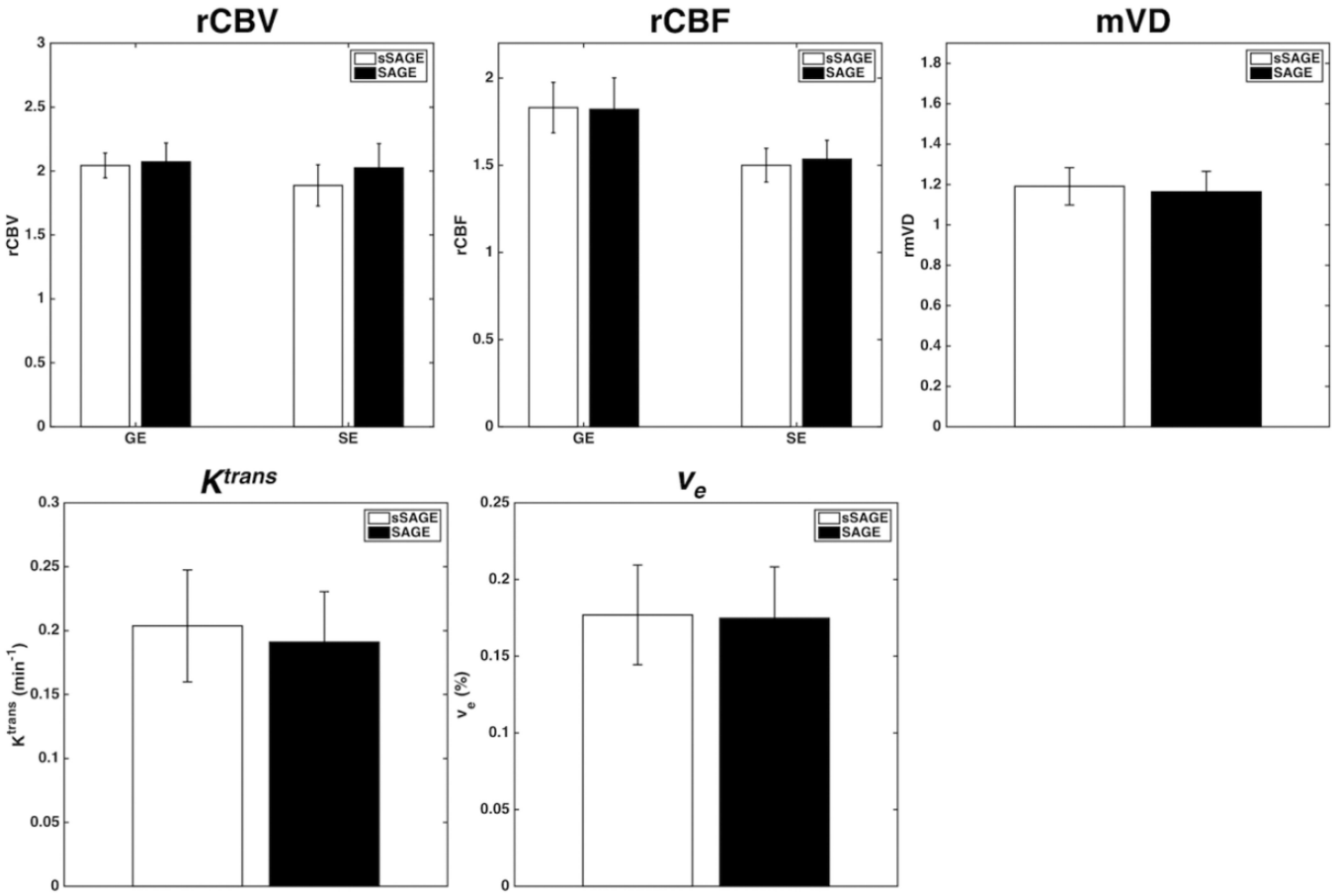

Figure 4.

Top: Bar plots showing mean GE and SE CBV, GE and SE CBF, and mVD relative to normal tissue for the sSAGE and SAGE methods. Bottom: Bar plots showing mean K^{trans} and v_e for the sSAGE, and SAGE methods. There were no significant differences between sSAGE and SAGE ($p>0.05$, $n = 8$).

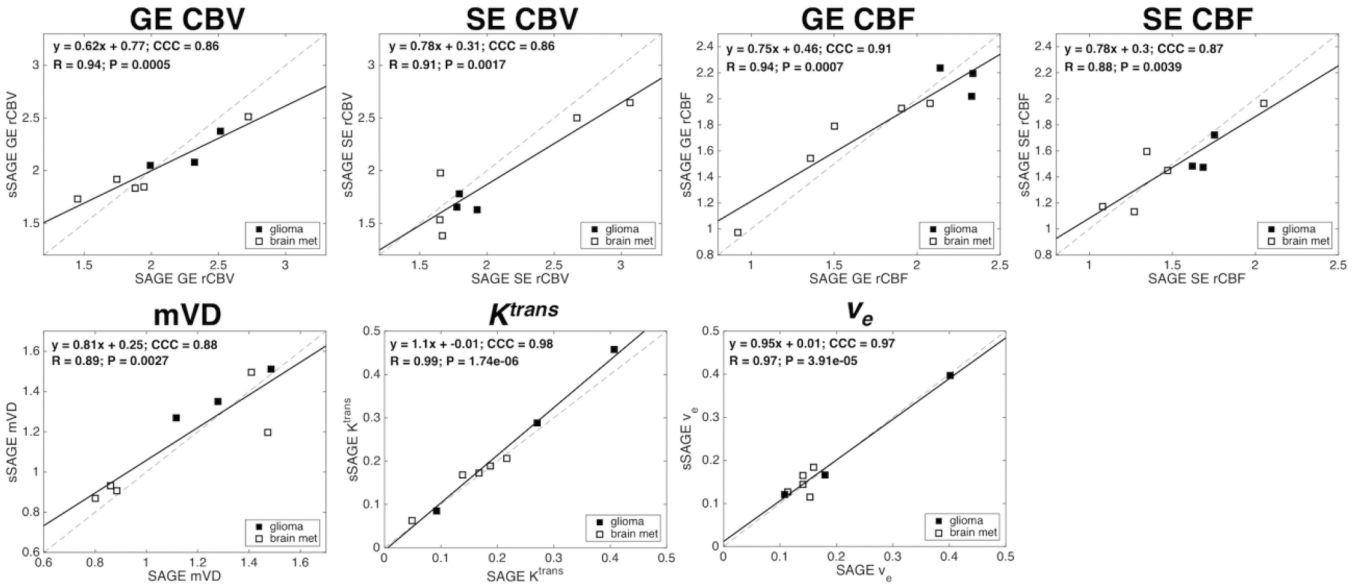

Figure 5.

Scatter plots showing mean GE and SE rCBV, GE and SE rCBF, mVD, K^{trans} and v_e from sSAGE and SAGE across all patients (n = 8; brain met patients are indicated by open markers). The linear regressions (slope and intercept, CCC, R and p-value) are shown for each plot, with significant correlations for each parameter.

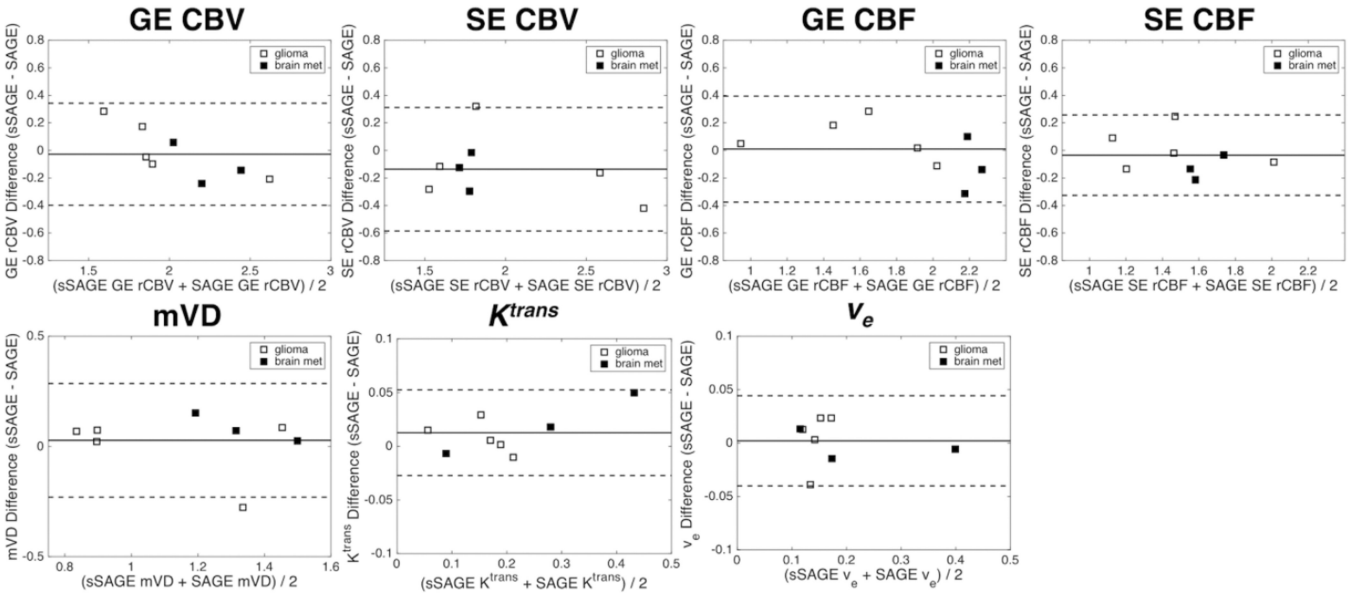

Figure 6.

Bland-Altman plots comparing sSAGE and SAGE GE and SE rCBV, GE and SE rCBF, mVD, K^{trans} and v_e in glioma (closed markers) and brain metastases (open markers) patients. There was minimal bias for each parameter (as determined by the average difference between the sSAGE and SAGE estimates).

Table 1

Patient demographics and Pearson's correlation coefficient (R) with SAGE

Patients: Primary Glioma	**Age**	**Sex**	**Pathology**	**Pearson's correlation (R) with SAGE (tumor ROI)**		
				sSAGE ΔR_2^*	**sSAGE ΔR_2**	**sSAGE T_1-w**
1	51	Male	Grade IV glioblastoma	0.97	0.95	0.98
2	55	Male	Grade III oligodendroglioma	0.92	0.88	0.94
3	42	Female	Grade IV glioblastoma	0.96	0.94	0.88
Patients: Metastatic Tumors	**Age**	**Sex**	**Primary tumor site**	**Pearson's correlation (R) with SAGE (tumor ROI)**		
				sSAGE ΔR_2^*	**sSAGE ΔR_2**	**sSAGE T_1-w**
1	62	Female	Lung - non-small cell	0.97	0.95	0.95
2	57	Male	Lung - non-small cell	0.81	0.87	0.80
3	72	Female	Melanoma	0.94	0.86	0.92
4	52	Female	Unknown	0.98	0.93	0.93
5	47	Male	Melanoma	0.78	0.78	0.75
			Mean:	**0.92**	**0.90**	**0.89**